Understanding the Atmospheric Temperature Adjustment to CO_2 Perturbation at the Process Level

YUWEI WANG AND YI HUANG

Department of Atmospheric and Oceanic Sciences, McGill University, Montreal, Quebec, Canada

(Manuscript received 15 January 2019, in final form 7 August 2019)

ABSTRACT

Climate model comparisons show that there is considerable uncertainty in the atmospheric temperature response to CO_2 perturbation. The uncertainty results from both the rapid adjustment that occurs before SST changes and the slow feedbacks that occur after SST changes. The analysis in this paper focuses on the rapid adjustment. We use a novel method to decompose the temperature change in AMIP-type climate simulation in order to understand the adjustment at the process level. We isolate the effects of different processes, including radiation, convection, and large-scale circulation in the temperature adjustment, through a set of numerical experiments using a hierarchy of climate models. We find that radiative adjustment triggers and largely controls the zonal mean atmospheric temperature response pattern. This pattern is characterized by stratospheric cooling, lower-tropospheric warming, and a warming center near the tropical tropopause. In contrast to conventional views, the warming center near the tropopause is found to be critically dependent on the shortwave absorption of CO_2. The dynamical processes largely counteract the effect of the radiative process that increases the vertical temperature gradient in the free troposphere. The effect of local convection is to move atmospheric energy vertically, which cools the lower troposphere and warms the upper troposphere. The adjustment due to large-scale circulation further redistributes energy along the isentropic surfaces across the latitudes, which cools the low-latitude lower troposphere and warms the midlatitude upper troposphere and stratosphere. Our results highlight the importance of the radiative adjustment in the overall adjustment and provide a potential method to understand the spread in the models.

1. Introduction

Considerable uncertainty remains in the projection of future climate change by the current global climate models (IPCC 2013). The magnitude of global warming can be diagnosed with a forcing-feedback framework (Ramaswamy et al. 2001), from which it can be recognized that the temperature projection uncertainty results from the uncertainties in both climate feedback, for example, that of clouds (Cess et al. 1990; Vial et al. 2013), and radiative forcing (Zhang and Huang 2014; Soden et al. 2018).

Concerning the forcing uncertainty, special attention needs to be given to the ''forcing adjustment.'' Forcing adjustment refers to the atmospheric adjustment that directly responds to the perturbation of a radiative agent, such as CO_2, without involving the warming in the sea surface temperature (SST) (Hansen et al. 1997). It is recognized that such adjustment induces a substantial subsequent change in the radiation energy budget and significantly modifies the magnitude of global radiative forcing (Zhang and Huang 2014). On the other hand, the atmospheric and land surface temperature changes that are categorized as ''adjustment'' constitute a substantial fraction of the overall global warming signal, especially in the stratosphere. Figure 1 shows the temperature adjustments in response to CO_2 quadrupling, obtained from a fixed-SST experiment in phase 5 of the Coupled Model Intercomparison Project (CMIP 5) (Taylor et al. 2012), and reveals substantial intermodel discrepancies in the temperature adjustment. The large discrepancy is noticed especially in the tropical tropopause region, where even the sign of the adjustment is uncertain. The adjusted radiative forcing also shows large spread in CMIP5, ranging from 6.22 to 8.63 $W m^{-2}$ in the estimation of Zhang and Huang (2014) and from 6.24 to 8.63 $W m^{-2}$ in Vial et al. (2013).

To narrow down the large uncertainty in the adjusted forcing, it is necessary to understand the basic mechanisms of the adjustment at the process level. The adjustment is a

Corresponding author: Yuwei Wang, yuwei.wang@mail.mcgill.ca

DOI: 10.1175/JCLI-D-19-0032.1

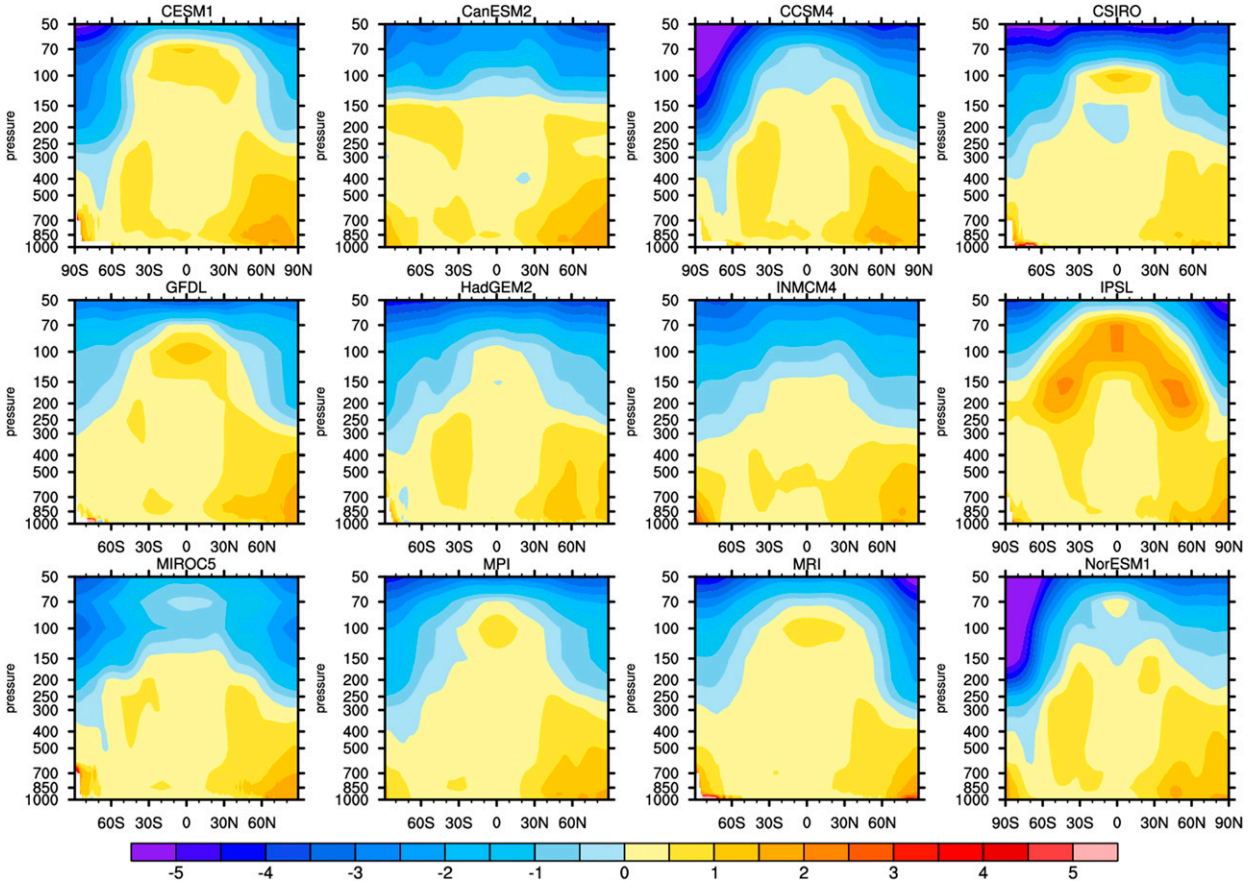

FIG. 1. The overall atmospheric temperature adjustment simulated by CMIP5 GCMs. The adjustment is measured by the difference in the mean temperature of the last 10 years between the sstClim4 × CO_2 and sstClim experiments in CMIP5. Unit: K.

combination of radiative, convective, and large-scale circulation effects. Among them, the instantaneous radiative forcing-induced adjustment can be considered a direct temperature response to the radiative heating rate perturbation caused by CO_2, which is termed "radiative adjustment" and distinguished from the adjustments resulted from nonradiative processes in this paper. The atmosphere and land surface adjust their temperatures to reinstate a balanced (nil) heating rate profile throughout the atmospheric column. Such a radiative adjustment inevitably leads to the change of the atmospheric static stability. The perturbed static stability results in a further convective adjustment of the vertical temperature profile. After the local temperature adjustments induced by the radiative and convective processes, the atmospheric circulation also needs to change in order to abide by the dynamical constraints, for example, the thermal wind relationship; this process may in turn further modify the temperature field. Following such a thought experiment, this work will study each of the processes successively. The aim of this work is to quantitatively assess how each of the processes drives the climate and improve the mechanistic understanding of the overall temperature change in adjustment.

Many efforts have been made to understand the global atmospheric temperature changes in the literature, for example, the application of the climate feedback response analysis method (CFRAM) (Lu and Cai 2009; Cai and Lu 2009). These works aimed at an attribution of the overall climate responses, for example, how the overall atmospheric and surface temperature changes simulated by climate models can be decomposed to partial changes due to factors such as CO_2 forcing and water vapor, cloud, and albedo feedbacks under energy balance constraints (e.g., Song et al. 2014). Such decompositions delineate how the temperature change happens in the models and quantitatively connects the overall temperature change to the contributing factors, essentially by solving the problem how much longwave radiation change is needed to balance the energy (or heating rate) perturbation induced by each factor. However, such decomposition does not explain how the energy perturbation associated with each factor arises in the first place.

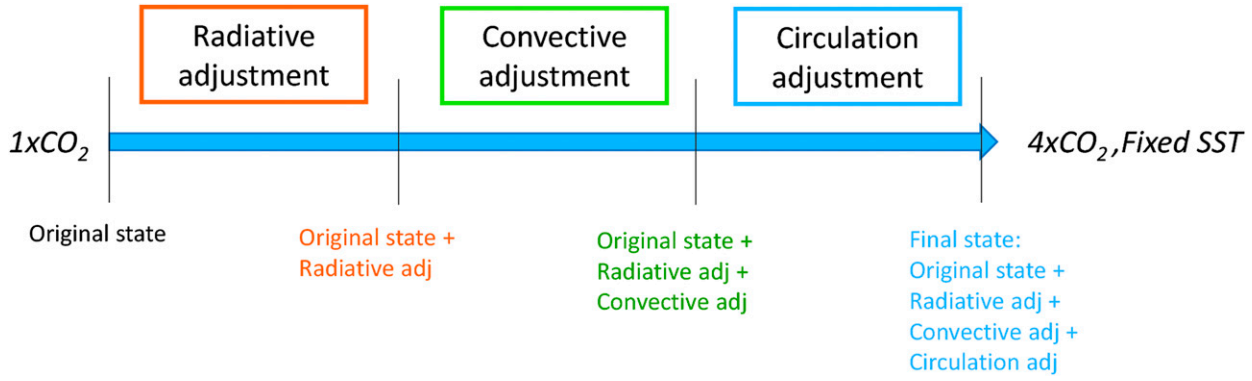

FIG. 2. Schematic illustration of the decomposition method and the terminology used in this study.

Here, we are motivated to address the problem differently, by identifying the climate responses that are driven by the different physical processes involved successively. Specifically, using a hierarchy of numerical climate models to simulate the temperature responses to CO_2 perturbation under different combinations of the processes in question (radiation, convection, and circulation), we aim at obtaining a global view of their individual effects on atmospheric temperature response. The novelty of our method is that we run models multiple times and add each of the processes successively (Fig. 2), so that how the climate evolves from the original state to the final state can be revealed. This work is similar in design to previous works, such as that of Lin et al. (2017), which aimed at identifying the mechanisms that drive regional (tropical tropopause) climate response. Readers are cautioned that the concepts of radiative adjustment, convective adjustment, and circulation adjustment may have different meanings when different decomposition methods are used. In the following section, we will define and explain the associated concepts in this study and describe the models we use and the experiments we design. We will then present and discuss the temperature changes due to each process and summarize our main findings in the end.

2. Model and method

We conduct a series of numerical experiments to delineate the effects of the processes involved on the atmospheric and surface temperature responses to CO_2 perturbation, which are summarized by the schematic of Fig. 2. First, we use a standard atmospheric general circulation model (GCM) to reproduce the control climate under $1 \times CO_2$ ($S\_1 \times CO_2$). Second, we use the radiative transfer model that is consistent with that in GCM to evaluate the radiative adjustment to $4 \times CO_2$ ($R\_4 \times CO_2$). Third, a single-column model that has the same physics package with the GCM is used to simulate the radiative–convective adjustment to $4 \times CO_2$ ($RC\_4 \times CO_2$). Fourth, the standard GCM is used again to simulate the overall adjustment under $4 \times CO_2$ where all the processes (radiation, convection, and circulation) are involved ($S\_4 \times CO_2$). The differences between these simulations allow us to isolate the temperature adjustments to the three processes. The radiative adjustment is defined as the second experiment minus the first experiment [$R\_4 \times CO_2 - S\_1 \times CO_2$]. The convective adjustment is the third minus the second [$RC\_4 \times CO_2 - R\_4 \times CO_2$], and the circulation adjustment is the fourth minus the third [$S\_4 \times CO_2 - RC\_4 \times CO_2$]. The overall adjustment is the fourth minus the first [$S\_4 \times CO_2 - S\_1 \times CO_2$], which is consistent with the overall climate response presented in Fig. 1. The details of the configuration of the models and the design of the experiments are described in the following.

a. Climate models

1) GCM

The full GCM used to simulate the overall temperature adjustment is the Community Atmosphere Model 5 (CAM5), together with the Community Land Model 4 (CLM4). The prescribed SST and sea ice concentration are from the Merged Hadley-NOAA/OI Sea Surface Temperature and Sea ice Concentration (Hurrell et al. 2008). Although ice fraction and ice depth are fixed, the ice temperature is free. CAM5 is configured with a T42 (roughly 3°) horizontal resolution. There are 30 vertical levels with the model top at around 3 hPa. The model uses the RRTMG radiation scheme, the University of Washington shallow convection scheme, and the Zhang–McFarlane deep convection scheme. All the other configurations are set as default (Eaton 2011).

2) RADIATION MODEL

The radiation model used for isolating the radiation effect is RRTMG (Clough et al. 2005), which is used in CAM5 as the default module. Instead of running RRTMG offline, which may introduce truncation errors and require large storage space, we have modified the CAM5 source codes to implement a ''double radiation call'' scheme. At each time step of CAM5 integration, the radiation module is called twice: one for the standard simulation and the other for the radiative adjustment simulation that uses a different atmospheric profile (with perturbed CO_2 concentration). An additional temperature field integrated from atmospheric heating rate generated by the second call is recorded together with the standard model outputs. Bit-by-bit comparison verifies that the standard simulation reproduces the results of the original codes.

3) SINGLE-COLUMN MODEL

The single-column model employed to simulate the radiative–convective adjustment is the Single-Column CAM (SCAM) (Gettelman et al. 2019). The physics package of SCAM is identical to the standard CAM5. The dynamics package is not included, since the model simulates the climate in an isolated single column. In comparison to CAM5, SCAM needs to be prescribed with lateral boundary conditions. These boundary conditions provide a summary of the advective process, specified as the tendencies in temperature, water vapor, cloud and other species associated with advection. We obtain the boundary conditions from the history files generated from the CAM5 simulation.

4) DRY GCM

To validate the effect of circulation on temperature adjustment and especially distinguish it from the effect of convection, we simulate the climate response with all the moist processes suppressed, by modifying the standard CAM to a ''dry'' version of CAM, in which water vapor is removed. In this simulation, we turn off both the shallow and deep convections and suppress the evaporation from both the ocean and the land. We also remove the water vapor from the initial conditions. At each time step, we output and check the water vapor in the model to ensure the water vapor content received by the physics modules (except the radiation codes) is zero. Because the radiative effect of CO_2 is dependent on the water vapor (Wang and Ryan 1983), in order to retain the same radiative effects of CO_2 perturbation as in the other experiments we prescribe the monthly mean water vapor distribution in the radiation scheme.

b. Numerical experiments

1) OVERALL TEMPERATURE ADJUSTMENT

To simulate the overall temperature adjustment in response to CO_2 perturbation, we use CAM5 to conduct a control run ($1 \times CO_2$) prescribed with 367 ppmv CO_2 concentration, and a perturbation run ($4 \times CO_2$) with 1468 ppmv CO_2 concentration. The prescribed SST and sea ice concentrations are fixed to year 1990 using the monthly mean data. Both the control run and perturbation run are integrated for 40 years to ensure the model approaches equilibrium climates. We difference the last 10 years from the two runs to define the overall temperature adjustment.

2) RADIATIVE ADJUSTMENT

In the control simulation ($1 \times CO_2$), when the climate system approaches equilibrium state, the total heating rate is close to zero. This equilibrium condition can be expressed as

$$\overline{H_{\rm rad}(1\times CO_2)} + \overline{H_{\rm conv}(1\times CO_2)} + \overline{H_{\rm circ}(1\times CO_2)} = 0, \tag{1}$$

where $H_{\rm rad}$ is the radiative heating rate, $H_{\rm conv}$ is the convective heating rate and $H_{\rm circ}$ is the circulation (advective) heating rate. The overbar indicates long-term average. As we quadruple the CO_2 concentration in the atmosphere, the radiative heating rate $H_{\rm rad}$ changes immediately. To investigate how the radiation process by itself drives climate change, we fix the convective and advective heating, following the idea of fixed dynamical heating (FDH) (Fels et al. 1980). Note that fixed dynamical heating rate here means that $H_{\rm conv}$ and $H_{\rm circ}$ in the perturbed climate are identical to the control ($1 \times CO_2$) simulation at every time step (20 min), rather than fixing the heating rate to a constant number. The water vapor and cloud distributions used in the computing $H_{\rm rad}$ are also identical to the control simulation. When a new equilibrium is reached, Eq. (1) changes to

$$\overline{H_{\rm rad}(4\times CO_2)} + \overline{H_{\rm conv}(1\times CO_2)} + \overline{H_{\rm circ}(1\times CO_2)} = 0. \tag{2}$$

Comparing Eq. (2) to Eq. (1), the essence of the radiative adjustment is that the atmospheric and land surface temperature adjust themselves to compensate the heating rate change caused by perturbed CO_2, so that

$$\overline{H_{\rm rad}(T, 1\times CO_2)} = \overline{H_{\rm rad}(T + dT_{\rm rad}, 4\times CO_2)}. \tag{3}$$

We use the ''double radiation call'' method described above [2a(2)] to simulate the atmospheric and land temperatures $T + dT_{\rm rad}$ under the $4 \times CO_2$ conditions. In the standard simulation, $H_{\rm rad}(1 \times CO_2)$, $H_{\rm conv}(1 \times CO_2)$ and $H_{\rm circ}(1 \times CO_2)$ are generated as in the normal CAM5 integration. In a parallel radiative adjustment simulation, a second radiative call computes the radiative heating rate at quadrupled CO_2 concentration, $H_{\rm rad}(4 \times CO_2)$, which is combined with $H_{\rm conv}(1 \times CO_2)$ and $H_{\rm circ}(1 \times CO_2)$ to compute radiatively adjusted temperature field:

$$T^{i+1}(4 \times CO_2) = T^i(4 \times CO_2) + [H^i_{\rm rad}(4 \times CO_2) + H^i_{\rm conv}(1 \times CO_2) + H^i_{\rm circ}(1 \times CO_2)] \times \Delta t, \quad (4)$$

where i is the index of the time steps, and Δt is the time interval. In the adjustment computation, the SST is prescribed with the same values as in the CAM5 control run. The land surface temperature is diagnosed following

$$T_S(4 \times CO_2) = \{[\sigma \times T_S^4(1 \times CO_2) + {\rm LWDN}(4 \times CO_2) + {\rm SWNET}(4 \times CO_2) - {\rm LWDN}(1 \times CO_2) - {\rm SWNET}(1 \times CO_2)]/\sigma\}^{1/4}, \quad (5)$$

where $T_S(1 \times CO_2)$ is the surface temperature from the standard simulation. LWDN and SWNET are downward longwave radiation at surface and net shortwave flux at surface respectively. In this simulation, we treat the land surface as a blackbody when we convert the surface flux change to temperature change. The evapotranspiration is also directly influenced by the CO_2 concentration through adjusting the stomatal conductance. However, this effect is not radiative, thus not included in Eq. (5). With the double-call method, the radiative adjustment simulation is performed along with the CAM5 control run (the standard simulation). It is also run for 40 years, and we use the last 10 years to define the temperature change. The radiative adjustment, $dT_{\rm rad}$, is obtained as the temperature difference between the $1 \times CO_2$ condition [Eq. (1)] and the $4 \times CO_2$ condition [Eq. (2)].

Most previous studies on radiative adjustment used ''Offline'' method (Cai and Lu 2009; Conley et al. 2013). The advantages of ''Online'' method are multifold: 1) The radiation code used in the radiative adjustment is consistent with that in the control run. 2) The heating rate is computed at the same frequency as the control simulation. 3) The long integration allows us to account for the dependence of the heating rate perturbation on different atmospheric conditions as occur in the real climate. 4) The ocean–land distribution and land surface properties are realistic and identical to the control run. 5) Also avoided are numerical errors from interpolating the atmospheric data from the GCM grid to the radiation model grid.

3) RADIATIVE–CONVECTIVE ADJUSTMENT

Based on a similar equilibrium constraint to Eqs. (1) and (2) but considering the heating rate resulting from the radiative and convective processes together, we have

$$\overline{H_{\rm rad-conv}(T, 1 \times CO_2)} = \overline{H_{\rm rad-conv}(T + dT_{\rm rad-conv}, 4 \times CO_2)}. \quad (6)$$

The left side of Eq. (6) represents the summation of $\overline{H_{\rm rad}(1 \times CO_2)}$ and $\overline{H_{\rm conv}(1 \times CO_2)}$ in Eq. (1). SCAM is used to simulate the atmospheric temperatures under the $1 \times CO_2$ and $4 \times CO_2$ conditions respectively. The SCAM is prescribed by both the lower boundary condition (fixed SST) and the lateral boundary condition (heating rate from CAM5 dynamical core). The lateral boundary condition is archived from $1 \times CO_2$ CAM5 control simulation at each time step (20 min). The initial condition is also output from CAM5 and consistent with the boundary condition at the start time. The number of grid points is 8192 (64×128, at T42 resolution), so SCAM need to run 8192 times for all the points in each experiment. The prescribed SST and land properties—such as the land fraction, the land topography, and the land heterogeneity—in SCAM are identical to those in the full CAM simulation. The radiative–convective adjustment $dT_{\rm rad-conv}$ is obtained as the difference between these two simulations.

Ideally, one would run the radiative–convective adjustment simulations described above for a long period (e.g., 40 years, as in the CAM5 experiment to obtain the overall adjustment) to obtain the radiative–convective adjustment. However, this would require a prohibitive amount of boundary conditions to be archived in order to run SCAM. Instead, we conduct the radiative–convective adjustment simulations with the boundary conditions of two months from the CAM5 simulation. Specifically, the January and July of model year 40 from the CAM5 control ($1 \times CO_2$) simulation are used. Figure 3 (comparing the first two columns) shows that the SCAM-simulated transient climate change, which is driven by boundary conditions identical to the $1 \times CO_2$ and $4 \times CO_2$ CAM5 simulations, can reproduce the transient climate change simulated by CAM5.

Given that the time scale it takes to reach radiative–convective equilibrium is up to one year (Cronin and Emanuel 2013), a transient (one month) simulation does not fully predict what equilibrium adjustment the

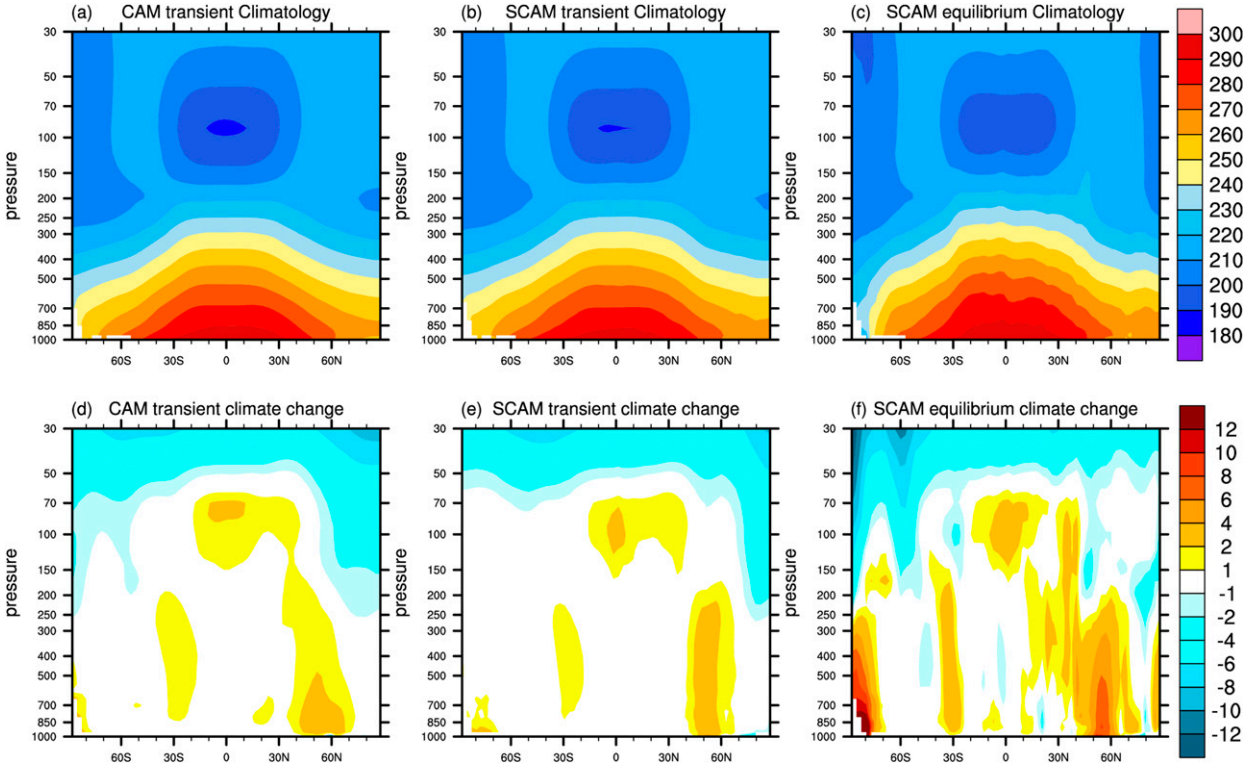

FIG. 3. (top) Mean climate and (bottom) temperature change simulated by CAM5 and SCAM. (a) CAM5-simulated average temperature of month January and month July of model year 40 under $1 \times CO_2$. (b) SCAM-simulated average temperature of the first month forced by the January lateral boundary condition and the first month forced by the July lateral boundary condition. (c) SCAM-simulated average temperature of the last 3 months of 2-yr simulations driven repetitively by the January and July lateral boundary conditions. (d)–(f) As in (a)–(c), but for temperature change between $4 \times CO_2$ and $1 \times CO_2$. Unit: K.

radiative–convective process would drive the climate to. To address this question, SCAM is integrated under the unperturbed (1×) and perturbed (4×) CO_2 concentrations, respectively, with repeated boundary conditions at the original time resolution (every 20 min) of each of these two months. Each integration (a total of four) is run for two years to ensure an equilibrium response is obtained. The equilibrium temperature adjustment of each month (January or July) is obtained by differencing the averages of the last three months of the 2-yr SCAM runs under the two CO_2 concentrations. The average of January and July is then used to represent the annual mean adjustment. Figure 3 (comparing the last column to the first) shows that the equilibrium radiative–convective adjustment simulated using this approximation scheme can reproduce the main features of the temperature adjustment simulated by CAM5. However, it is noticed that the SCAM simulation overestimates the temperature change magnitude, for example, the warming near the tropical tropopause, in the Northern Hemispheric midlatitudes and in the Southern Hemispheric polar regions. Recognizing this difference, when diagnosing the CAM5 simulation, we apply a scaling factor to normalize the temperature changes simulated by SCAM. The scaling factor is defined as follows:

$$S = \frac{Q\,\text{increase in SCAM}}{Q\,\text{increase in CAM}} = \frac{\dfrac{Q_{\text{SCAM\_4}\times\text{CO}_2} - Q_{\text{SCAM\_1}\times\text{CO}_2}}{Q_{\text{SCAM\_1}\times\text{CO}_2}}}{\dfrac{Q_{\text{CAM\_4}\times\text{CO}_2} - Q_{\text{CAM\_1}\times\text{CO}_2}}{Q_{\text{CAM\_1}\times\text{CO}_2}}}, \quad (7)$$

where Q is the globally averaged column-integrated specific humidity, which increases by 1.74% in CAM5 and 2.05% in SCAM simulations. So, the scaling factor is determined to be 1.18. We note that the scaling factor only tunes the mean amplitude of temperature response but has little impact on the identified temperature pattern (see the discussion in section 3c below).

The experiment design adopted here resembles that of the FDH experiments (Fels et al. 1980). In each experiment we only allow the processes of interest to respond to CO_2 forcing and suppress the change in heating rate due to other processes. When assessing radiative

adjustment, the convective and circulation heating rates are fixed. When assessing radiative–convective adjustment, the circulation heating rate is fixed. With the three temperature adjustments obtained as described above, we can derive the convective adjustment by subtracting the radiative adjustment [section 2b(2)] from the radiative–convective adjustment [section 2b(3)] [RC_4 × CO_2 − R_4 × CO_2], and the large-scale circulation adjustment by subtracting the radiative–convective adjustment [section 2b(3)] from the overall adjustment [section 2b(1)] [S_4 × CO_2 − RC_4 × CO_2].

3. Results

Figure 3 summarizes the zonally averaged overall temperature adjustment and the component adjustments due to the three processes, diagnosed using the method as described above. The overall adjustment simulated from CAM5 resembles the CESM result in Fig. 1. There is generally warming in the troposphere and a substantial cooling in the stratosphere. The largest warming occurs near the surface over the Arctic, with a value of more than 3 K. The near-surface air over Antarctica also shows a local warming maximum, although the warming layer is shallower. There is a warming center near the tropical tropopause, with a maximum value of around 2 K. In the following, we describe how this overall temperature change pattern results from the radiative, convective, and large-scale circulation adjustments, respectively.

a. Radiative adjustment

The radiative adjustment is shown in Fig. 4b. It shows an alternating pattern, warming in the middle and lower troposphere below 300 hPa and cooling above, except for the tropopause region around the 80 hPa extending from the equator to 50°S/N. Substantial cooling occurs in the stratosphere, reaching about −17 K at 3 hPa (model top). The tropical tropopause region warms by 2 K. The near-surface warming is about 3 K.

The radiatively driven temperature changes have been long known (e.g., Manabe and Wetherald 1967). Most of these changes can be explained by the atmospheric heating rate perturbation caused by CO_2. For instance, the stratospheric cooling and near-surface warming are explained respectively by the cooling-to-space and warming-through-the-exchange-with-surface components of radiative heating, both of which are enhanced by the increase of atmospheric CO_2 (Goody and Yung 1989).

The warming center near the tropical tropopause is worth some discussions as this is a region where the GCMs (see Fig. 1) differ noticeably. Both the longwave and shortwave heating of CO_2 may contribute to this feature. Previous studies (Thuburn and Craig 2002; McLandress et al. 2014; Lin et al. 2017) emphasized more on the longwave effect, which from the heating rate perspective dominates the initial temperature change when CO_2 is perturbed (see Fig. 5) due to the sharp curvature of the temperature profile near the tropopause. However, we find that the warming is critically dependent on the shortwave effect. This is demonstrated by a series of experiments, in which we perturb the CO_2 in longwave and shortwave radiation schemes respectively (longwave only, shortwave only, and both). Figures 5a and 5d show that the longwave effect is insufficient to cause this warming center. This is because although the longwave heating initially induces warming in this region, as the stratosphere cools, the longwave heating at this level changes from the positive to the negative. This reduction in longwave heating cannot be offset by the surface warming, which is verified by additional experiments in which the surface temperature is fixed or changed [according to Eq. (5)], respectively (not shown). This also explains why the warming is limited to the low- and midlatitude regions where the solar insolation is higher. If we check the radiative adjustment month by month, we can see the warming shifts with the maximum solar insolation (Fig. 6). We test the model dependence of the warming center using another two radiative transfer models, the line-by-line benchmark model (LBLRTM) and the Community Atmosphere Model Radiative Transfer model (CAMRT) (old version of radiation scheme in CAM3). Both models reproduce the warming near the tropopause, but with obvious different magnitudes. Details of the quantification and its impact on the model projections are discussed in Huang and Wang (2019).

Figure 7 shows the results from similar longwave-only and shortwave-only experiments using CAM5 (double radiation call) and confirmed the above finding (Fig. 5). For longwave effect, the radiative temperature adjustments show warming below 300 hPa and cooling above but no near-tropopause warming center. The shortwave effect has a nearly opposite pattern and explains the warming center near the tropical tropopause.

This result here suggests that the initial heating rate perturbation may not predict the end state of the temperature adjustment. The interactions between different atmospheric layers may eventually change the sign of the initial temperature perturbation. This also indicates that comparing the heating rate alone may not sufficiently validate a radiation model or explain the intermodel difference in their temperature projection.

Last, we note that the temperature change simulated here is obtained in an FDH context. This differs from the

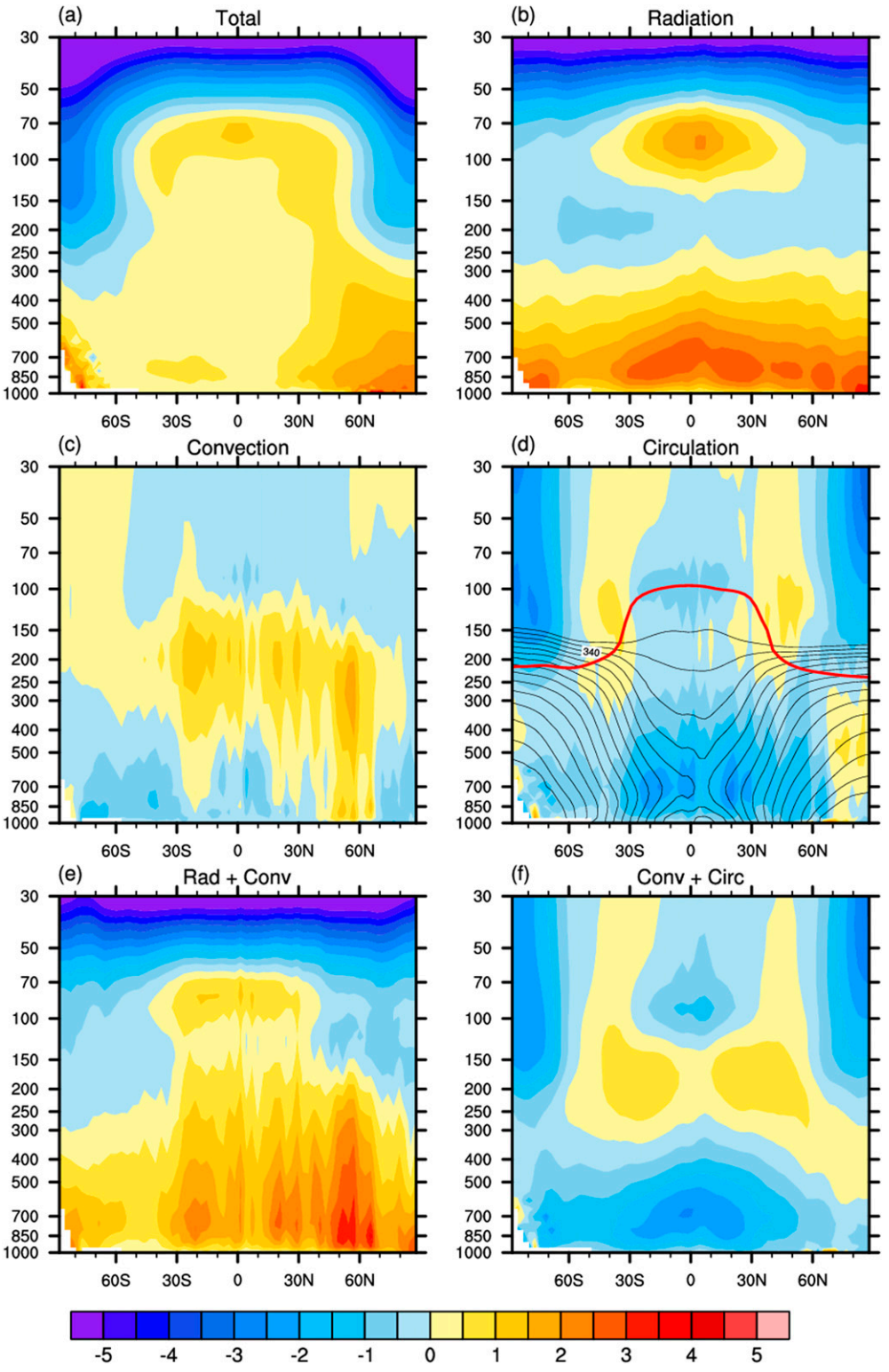

FIG. 4. Atmospheric temperature adjustments. (a) Total adjustment. (b) Radiative adjustment. (c) Convective adjustment, before applying the scaling factor. (d) Circulation adjustment. The black lines are equivalent potential temperatures. The red line is the tropopause following the criterion defined by WMO. (e) Radiative–convective adjustment, the temperature difference between the experiment of 4 × CO_2 configuration with 1 × CO_2 boundary condition and the experiment of 1 × CO_2 configuration with 1 × CO_2

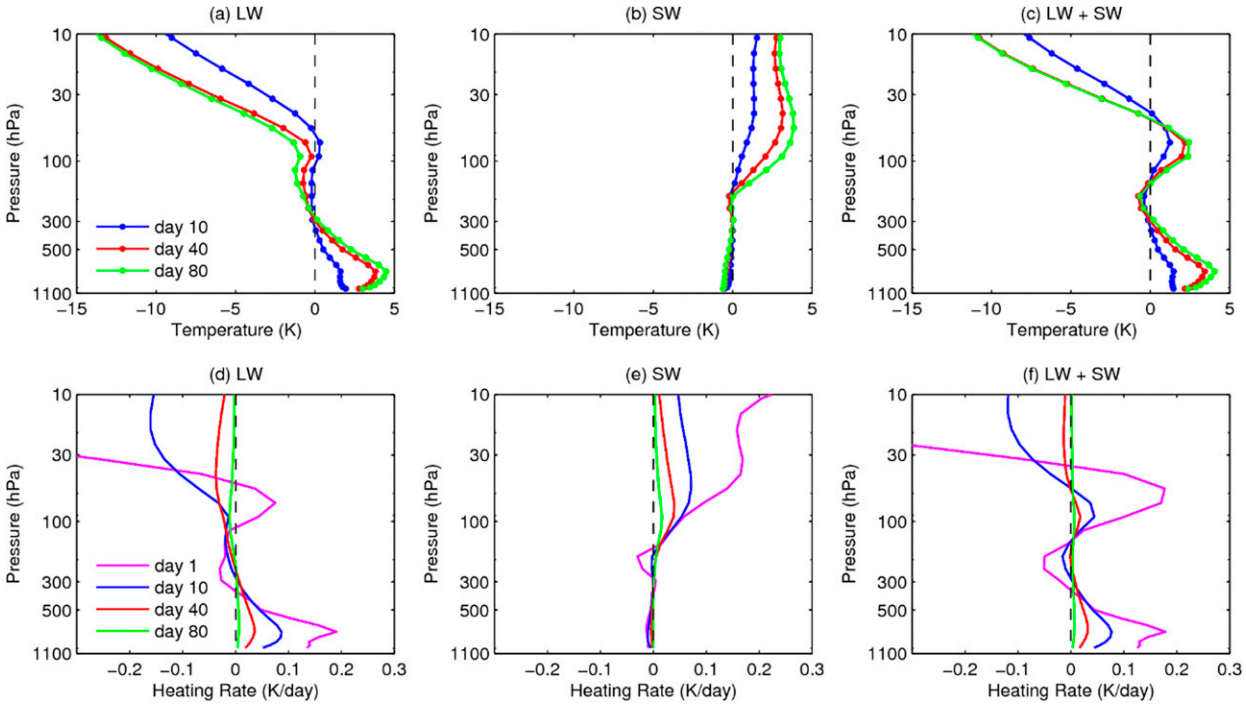

FIG. 5. Radiative adjustment simulated by 1D radiation model, RRTMG. (top) The evolution of temperature anomaly in the CO_2 perturbation experiments. (bottom) The corresponding radiative heating rate evolution. (a),(d) $4 \times CO_2$ in longwave (LW) radiation scheme and $1 \times CO_2$ in shortwave (SW) radiation scheme; (b),(e) $1 \times CO_2$ in longwave radiation scheme and $4 \times CO_2$ in shortwave radiation scheme. (c),(f) $4 \times CO_2$ in both longwave and shortwave radiation schemes.

radiative equilibrium context, where the atmosphere is perturbed from an equilibrium state of nil radiative heating rate (e.g., Manabe and Strickler 1964). The base (unperturbed) climate of such a radiative equilibrium is much different from the realistic climate that the adjustment simulation here begins with. Because of this difference, we argue the simulation here is more relevant. Nevertheless, Fig. 8 shows that the temperature changes simulated in these two contexts are very similar.

b. *Convective adjustment*

Subtracting the radiative adjustment described above from the radiative–convective adjustment simulated by SCAM, we obtain a measure of the convective effect on the atmospheric temperature. Figure 9 shows the convective adjustments for January, July, and their average. Convection is enhanced under the quadrupled CO_2 due to the decrease of the static stability. The potential temperature increases in the lower troposphere and decreases in the upper troposphere due to the radiative adjustment, which makes the atmosphere less stable and possess more convective available potential energy (CAPE). As a result, more heat is transported from the lower troposphere to the upper troposphere. The warming center of the convective adjustment is around 200 hPa, with maximum value around 2 K in the average (Fig. 9c). The convective adjustment is stronger in July than in January. The adjustment is also not uniform latitudinally, with the tropics and Northern Hemispheric midlatitudes showing more significant changes. There is warming throughout the troposphere over the Northern Hemispheric midlatitudes.

Compared to the radiative adjustment, the magnitude of the convective adjustment is smaller (cf. Figs. 4b and 4c). It is interesting to note that the convective adjustment induces opposite temperature changes to the radiative adjustment. The radiative adjustment warms the lower troposphere and cools the upper troposphere, while convective adjustment warms the upper troposphere and cools the lower troposphere.

←

boundary condition in SCAM. The temperature difference is averaged between January and July. (f) Convective plus circulation adjustment, obtained by subtracting the radiative adjustment from the total adjustment. Unit: K.

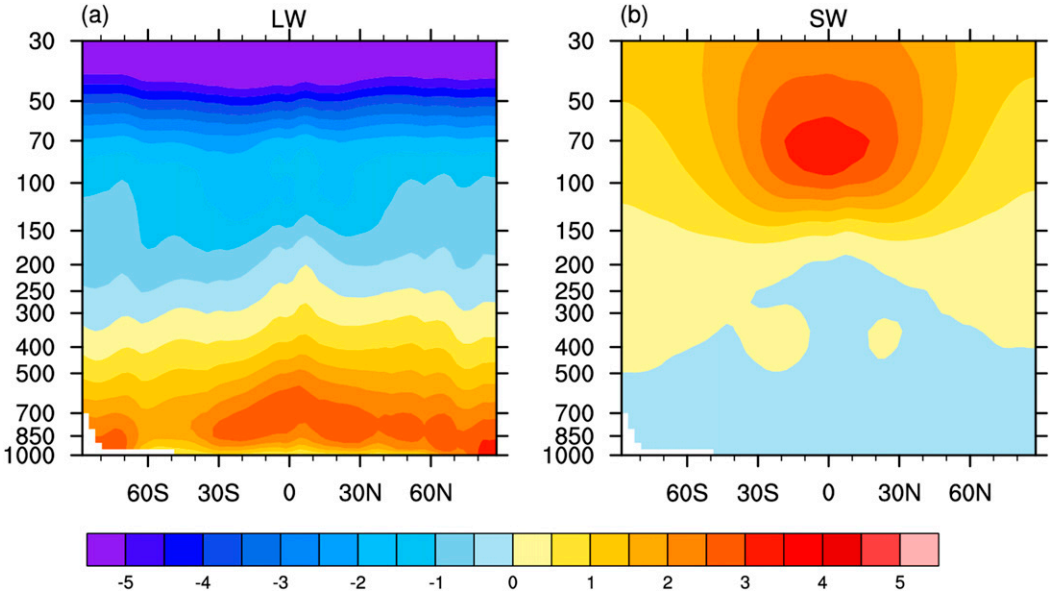

FIG. 6. Longwave- and shortwave-only radiative adjustment simulations, as in Figs. 4a and 4b, conducted using the double-radiation call scheme in CAM5. Unit: K.

The opposite effects of radiative adjustment and convective adjustment can also be seen in the heating rate change. Figure 10 shows the heating rate differences between $4 \times CO_2$ and $1 \times CO_2$ at the beginning and the end of the simulations at an ocean grid in west Pacific. In contrast to the radiative adjustment where the radiative heating perturbation diminishes at the end of the adjustment, the radiative heating rate in the radiative–convective adjustment only weakens. The nonzero radiative heating rate is largely balanced by the convective heating rate, leading the net heating rate to close to zero. Figure 11 is the zonal mean heating rate changes between the $4 \times CO_2$ and $1 \times CO_2$ conditions. The radiative effect shows a warming in the lower troposphere and cooling in the upper troposphere, while the convective heating rate change shows the opposite.

The radiative–convective adjustment warms the troposphere and cools the stratosphere (Fig. 4e). Compared to the overall temperature adjustment (Fig. 4a), it reproduces the stratosphere cooling, the tropopause warming and the polar warming. However, the warming in the lower troposphere in the tropics and midlatitudes is stronger than in the overall temperature adjustment, indicating circulation adjustment may play an important role there.

c. *Circulation adjustment*

The effect of large-scale circulation on temperature adjustment is obtained by subtracting the radiative and convective adjustments (Figs. 4a,b) from the total adjustment (Fig. 4d). As discussed in section 2d, SCAM, as it runs toward equilibrium, overestimates the convective adjustment simulated in CAM5 experiment. So, we normalize the convective adjustment by dividing it with the aforementioned scaling factor 1.18 [obtained from Eq. (3)] when computing the circulation adjustment:

$$dT_{\text{circ}} = dT_{\text{total}} - dT_{\text{rad}} - \frac{dT_{\text{conv\_scam}}}{1.18}. \tag{8}$$

The circulation adjustment pattern disclosed by Fig. 4d indicates an isentropic redistribution of the heat. The black lines are the equivalent potential temperatures. The circulation adjustment cools the lower troposphere, especially in the low latitudes, and warms the midlatitude upper troposphere and stratosphere as well as the upper troposphere over Arctic. The largest cooling (about −3 K) occurs in the tropical lower troposphere where major radiative heating occurs (Fig. 4b), indicating that the circulation adjustment also has an opposite effect to the radiative adjustment. The warming in the lower troposphere driven by the radiative adjustment is transported from the lower troposphere to upper troposphere through the equivalent potential temperatures. We have tested the sensitivity of the circulation adjustment to the scaling factor. All the features are qualitatively robust except for the tropical upper troposphere (30°S–30°N, 250–150 hPa). The tropical upper troposphere could be slightly warming if the scaling factor is set to be a large value, such as 2.

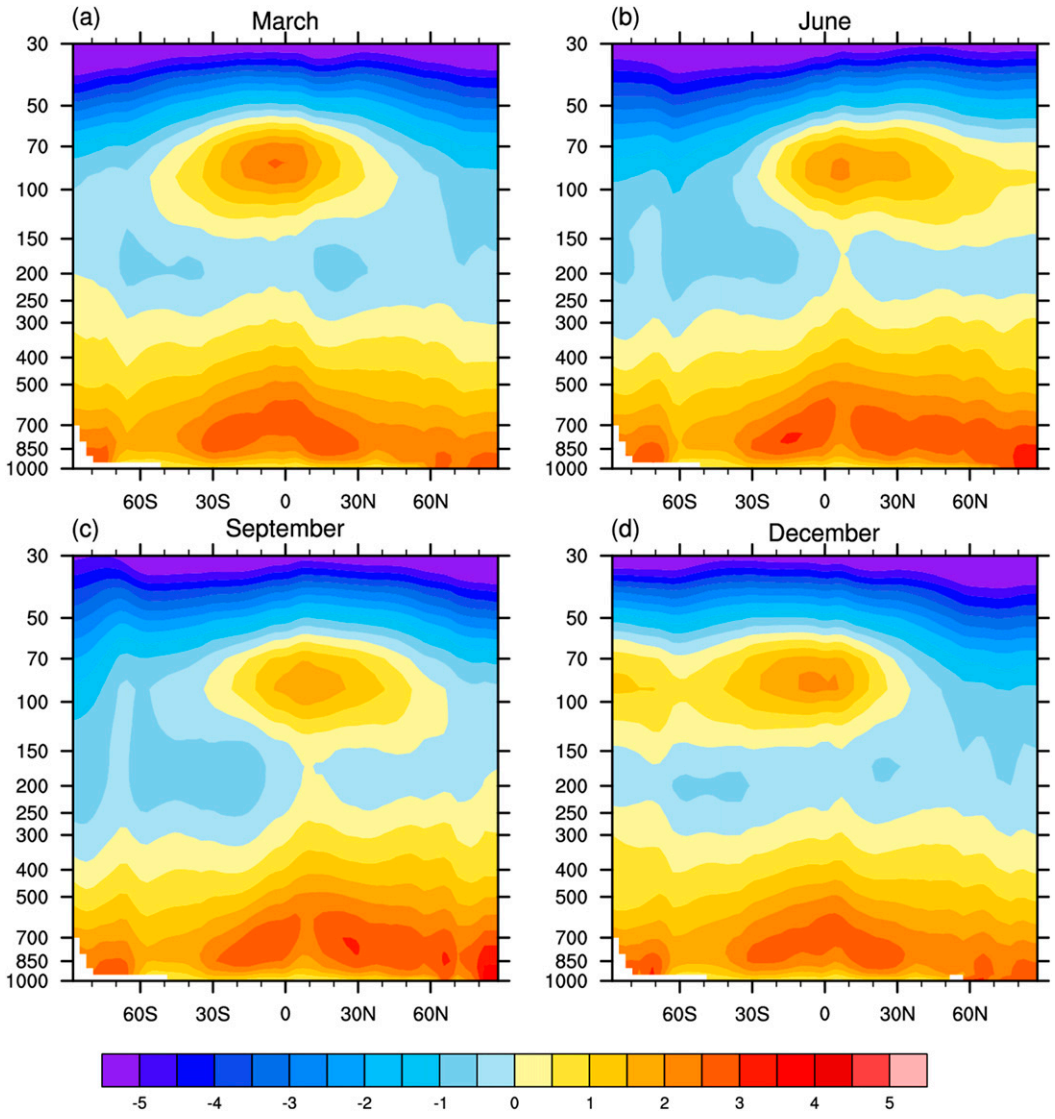

FIG. 7. Warming near the tropopause shifts in different months. Unit: K.

The temperature change pattern in Fig. 4d also suggests a possible contribution by the circulation adjustment to the polar amplification phenomenon. The advective transport of heat from the tropical lower troposphere to the extratropical upper levels results in a near-surface meridional gradient in temperature distribution, which corresponds to the stronger overall warming in the Arctic in the overall temperature adjustment (Fig. 4a). As shown by Fig. 1, the polar amplification is a robust feature in all models even though the SSTs are prescribed in this experiment (sstClim4 × CO_2). With regard to the average of all models shown in Fig. 1, the near-surface atmospheric temperature over Arctic increases by 1.8 K, in comparison to a 0.2 K at the equator. Compared to the full warming of 14.1 K in the Arctic (4.7 K in the equator) in the abrupt4 × CO_2 experiment (which includes the feedback effects), the overall adjustment accounts for 12.4% of the Arctic warming (4% of the equator warming). The temperatures of full warmings are averaged for the last 10 years at the end of 150-yr simulations in abrupt4 × CO_2 experiments.

To further verify the circulation effect on atmospheric temperature, we conduct an experiment with the dry-CAM model. Circulation and convection strongly interact with each other. In dry-CAM where moist processes are suppressed, we can clearly identify the circulation effect from the convective effect. The circulation directly responds to the radiative adjustment, avoiding the interference of the convection.

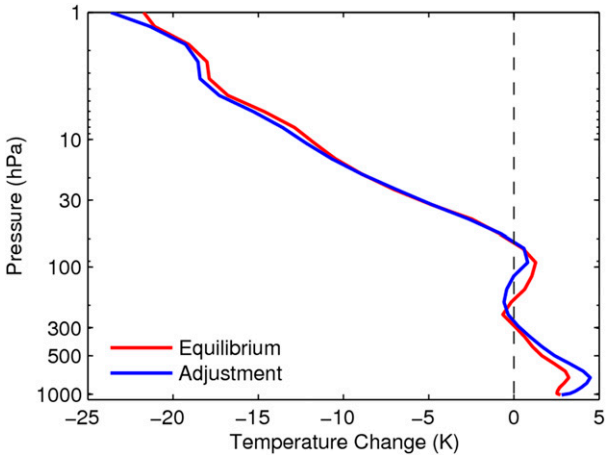

FIG. 8. Temperature changes driven by the radiative process alone, in the context of radiative equilibrium and radiative adjustment, respectively. The simulation is based on the equatorial zonal mean profile (averaged between 2.5°S and 2.5°N) in the 1 × CO_2 control experiment. The temperature change in the radiative adjustment case is simulated according to Eq. (4) (under the fixed dynamical heating assumption); that in the radiative equilibrium case is the difference in radiative equilibrium temperatures between the 1 × CO_2 and 4 × CO_2 conditions.

As shown by Fig. 12, the model simulates a climatology similar to CAM5. The overall temperature adjustment also warms the troposphere and cools the stratosphere. However, without convection, the warming is stronger in the lower troposphere in the tropics and Northern Hemispheric midlatitudes, where convection shows a significant cooling effect in the full CAM simulation (Fig. 13b). The radiative adjustment resembles that in CAM5. As the convective effect is suppressed in dry-CAM, the circulation adjustment is obtained by subtracting the radiative adjustment from the overall adjustment. The circulation adjustment rendered by dry-CAM (Fig. 12d) affirms an isentropic heat redistribution disclosed by the previous diagnosis (Fig. 4d), although the warming in the middle and upper troposphere is more pronounced and continuous. The circulation adjustment in dry-CAM resembles the convective plus circulation adjustment in full CAM5(Fig. 4f). We note that the convective effect termed in this paper represents the effect of the upright convections, while the slantwise convections, which are active in the extratropics (e.g., Chen et al. 2018) and account for the moisture transport to the Arctic (Laliberté and Kushner 2013; Merlis and Henry 2018), are categorized as a circulation effect. The resemblance between Fig. 12d and Fig. 4f suggests that the convective and circulation effects on temperature are complementary to each other, acting together to offset the effect of the radiative adjustment on the vertical temperature structure, especially the destabilization of the free troposphere above the boundary layer (Figs. 4c and 12b). This notion is also supported by the heating rate decomposition. The convective heating rate change in radiative–convective experiment (Fig. 11b) and the circulation heating rate change in dry-CAM experiments (Fig. 12f) both yield similar effects to the convective plus circulation heating rate change in full CAM simulations (Fig. 13d). The circulation adjustment in the stratosphere (Figs. 4d and 12d) resembles the ''bullhorn'' pattern shown by Huang et al. (2016), which can be attributed to the strengthening of Brewer–Dobson circulation (Lin and Fu 2013).

Last, we note that the atmospheric heating rate components in the full GCM (Fig. 13) cannot fully predict the temperature adjustments driven by respective processes: radiation, convection and circulation (Fig. 4).

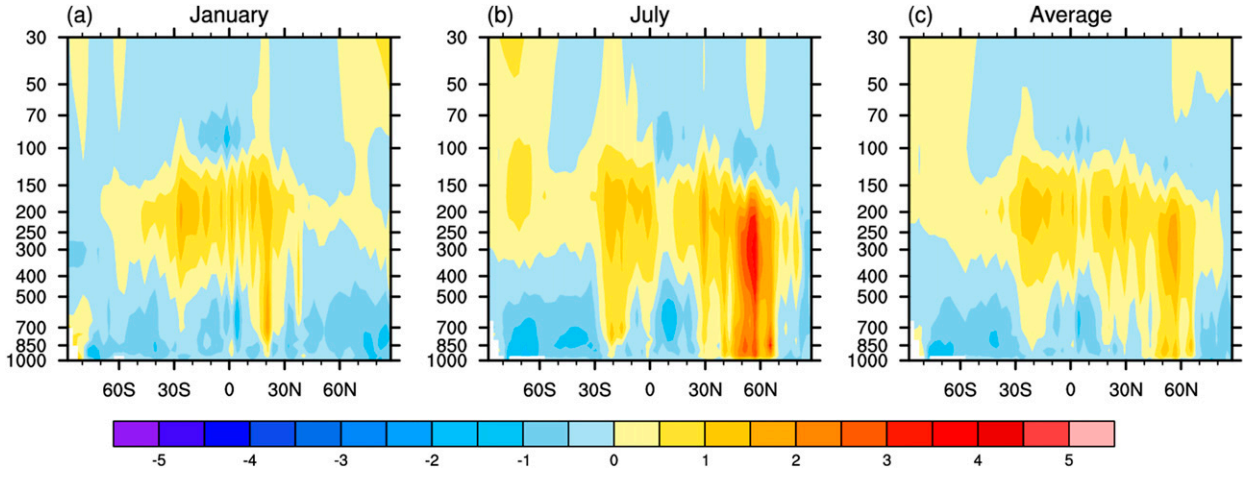

FIG. 9. Convective adjustment simulated in (a) January, (b) July, and (c) their average. Unit: K.

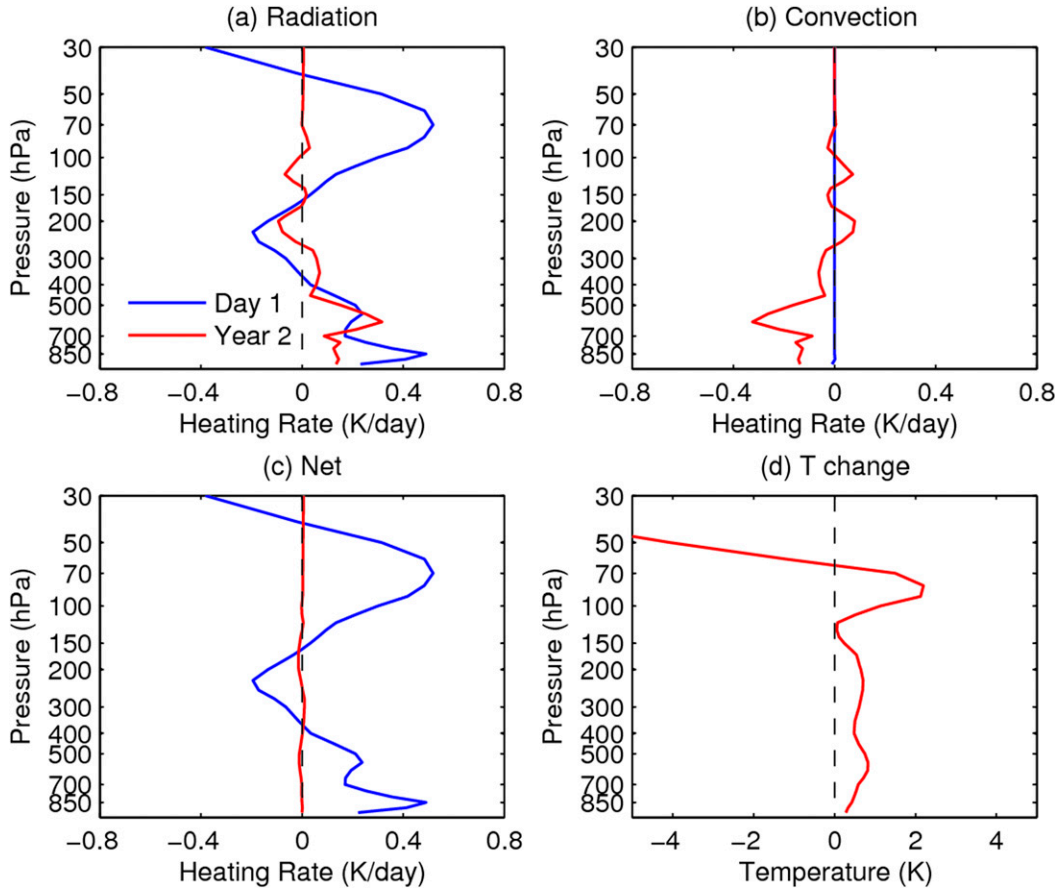

FIG. 10. SCAM-simulated heating rate changes and temperature change between 4 × CO_2 and 1 × CO_2 experiments at an ocean grid (10°N, 152°E). The results are averaged between the January and the July simulations. The blue and red lines show the changes at the beginning and at the last 3 months of 2-yr simulations, respectively. (a) Radiative heating rate change, (b) convective heating rate change, (c) net (radiative plus convective) heating rate change, and (d) temperature change.

One reason leading to such lack of correspondence is that the three processes are coupled in the full GCM. For instance, the convective and circulation effects may change atmospheric composition (e.g., water vapor and clouds, as discussed above) and consequently the radiative heating rate. Similarly, the moisture redistributed by the circulation effect may subsequently affect the convective heating rate. As a result, it is evident from Figs. 13b–d that the heating rate changes associated with some processes, for example, the parameterized convection and resolved advection (circulation effect), are noisy (of fine spatial structures) and anticorrelated, as they collectively serve to counteract the effect of the radiative adjustment on temperature structure. Because of these reasons, it should be cautioned that attribution based on heating rate decomposition may have limitations in disclosing how each process drives the atmospheric adjustment.

We further use the kernel method to estimate the impact of temperature change on the adjusted forcing. Following the method introduced by Zhang and Huang (2014) and using the CAM3 kernel (Shell et al. 2008), we calculate the adjusted forcing at each grid box and then integrate vertically and average over the globe. The overall temperature adjustment, including both atmospheric and surface temperature adjustments, induces a global-mean all-sky TOA forcing of 0.18 $W m^{-2}$, close to the mean value in CMIP5 models estimated by Zhang and Huang (2014, see their Table 1). The atmospheric temperature adjustment alone accounts for 0.61 $W m^{-2}$, which can be decomposed to a radiative adjustment of −1.42 $W m^{-2}$, a convective adjustment of −0.12 $W m^{-2}$, and a circulation adjustment of 2.15 $W m^{-2}$. The radiative adjustment results in a negative forcing due to the considerable warming in the troposphere whose effect on the TOA radiation exceeds that of the cooling in the stratosphere. The

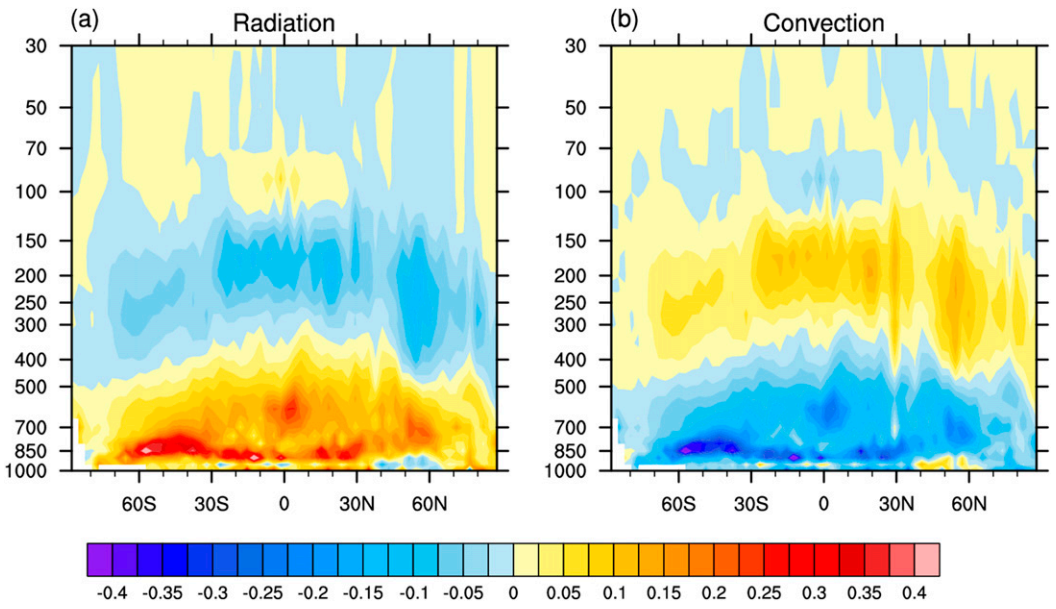

FIG. 11. SCAM-simulated zonal mean heating rate changes between $4 \times CO_2$ and $1 \times CO_2$ experiments. The results are averaged between the January experiment and the July experiment. Unit: K day^{-1}.

positive forcing of the circulation adjustment is due to the cooling it induces in the troposphere.

4. Conclusions

Inter-GCM comparisons disclose large uncertainties in the atmospheric temperature response to CO_2 perturbation even when the GCMs are prescribed with identical SST and sea ice (Fig. 1). We conduct a series of numerical experiments to understand how the atmospheric temperature change arises from the CO_2 perturbation. Using a full GCM (CAM5) and its associated radiation model and single-column model, we identify the temperature adjustments driven by the radiative, convective and circulation effects, respectively (Fig. 4). These effects can be summarized as follows:

1) The radiative adjustment leads to cooling in the stratosphere, warming in the troposphere below 300 hPa and a warming center around the tropical tropopause region (Fig. 4b). In contrast to the conventional views, we find this tropical tropopause warming center to be critically dependent on the shortwave absorption of CO_2 (Figs. 5–7).
2) The convective adjustment cools the lower troposphere and warms the upper troposphere (Fig. 4c). This effect generally counteracts the effect of the radiative adjustment.
3) The circulation adjustment largely redistributes the energy along the isentropic surfaces (Fig. 4d). It cools the lower troposphere, especially in the tropics, and warms the upper troposphere and stratosphere in the extratropics including the Arctic (Fig. 4d). A dry-CAM simulation (Fig. 12), which removes the nonradiative moisture effects, confirms the isentropic redistribution of the energy by the dynamics and indicates there is complementarity between the effects of local (upright) convection and large-scale circulation.

In summary, the overall temperature adjustment can be understood as the radiative effect changes the atmospheric temperature in such a way that the tropospheric static stability is reduced while the convective and circulation adjustments largely counteract the radiative effect by redistributing the energy largely along the isentropic surfaces and restabilizing the atmosphere. The results here highlight the importance of the radiative process that triggers all the adjustments and thus draw attention to the inaccuracy of radiation codes, which may have led to the discrepancies in the temperature adjustment simulated by different GCMs (Fig. 1) and shall be investigated in the following work. On the other hand, there may be complex coupling between different vertical portions of the atmosphere (as illustrated by Fig. 5) or between different processes that jointly drive the atmospheric adjustment (as disclosed by the complex heating rate components in Fig. 9), which should be kept in mind while interpreting

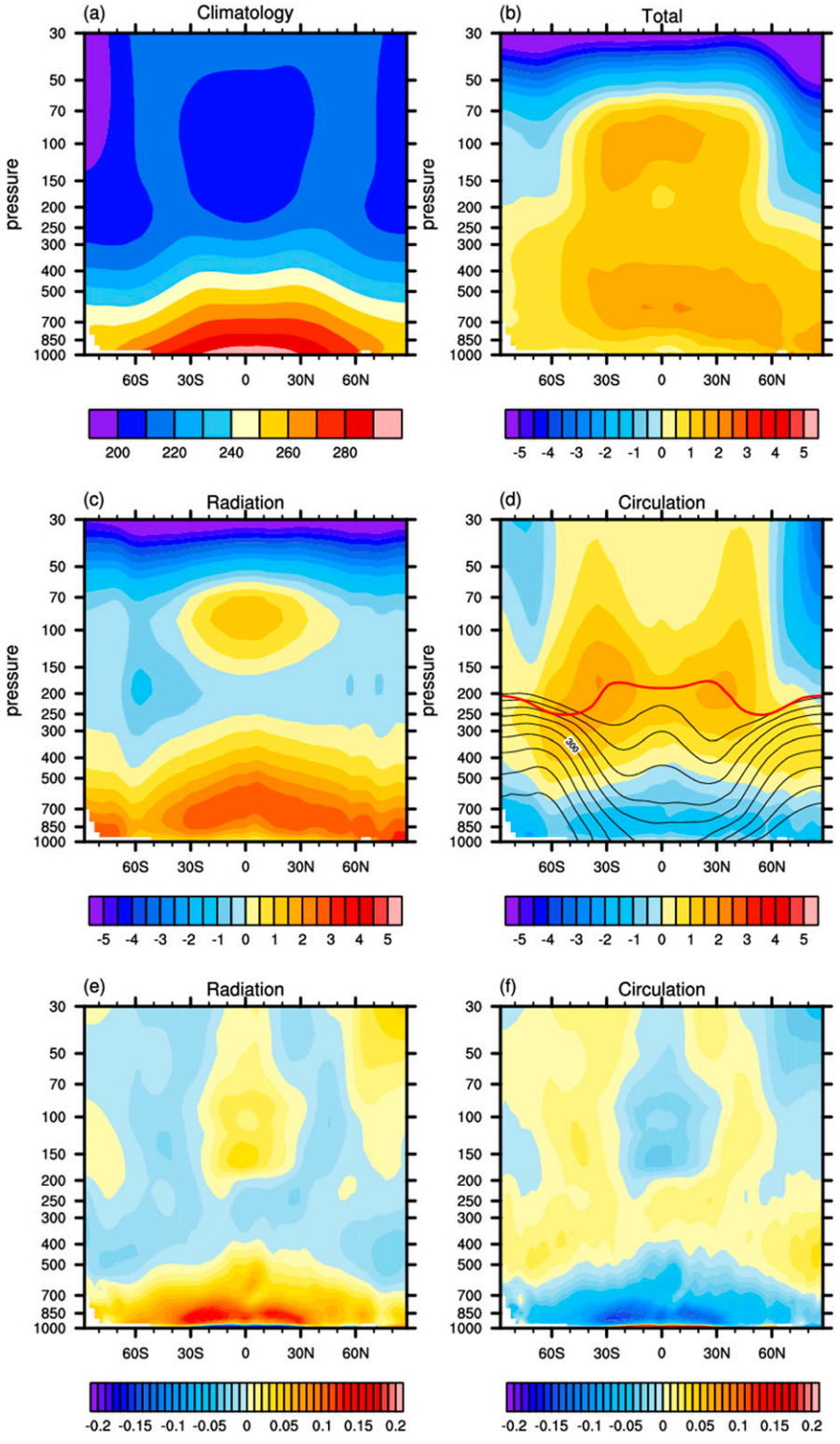

FIG. 12. Dry-CAM simulations. (a) Zonal mean temperature climatology under $1 \times CO_2$. Unit: K. (b) Total temperature adjustment. Unit: K. (c) Radiative temperature adjustment. Unit: K. (d) Circulation temperature adjustment. Unit: K. The black lines are potential temperatures. The red line is the tropopause following the criterion defined by WMO. (e) Radiative heating rate change. Unit: K day^{-1}. (f) Circulation heating rate change. Unit: K day^{-1}.

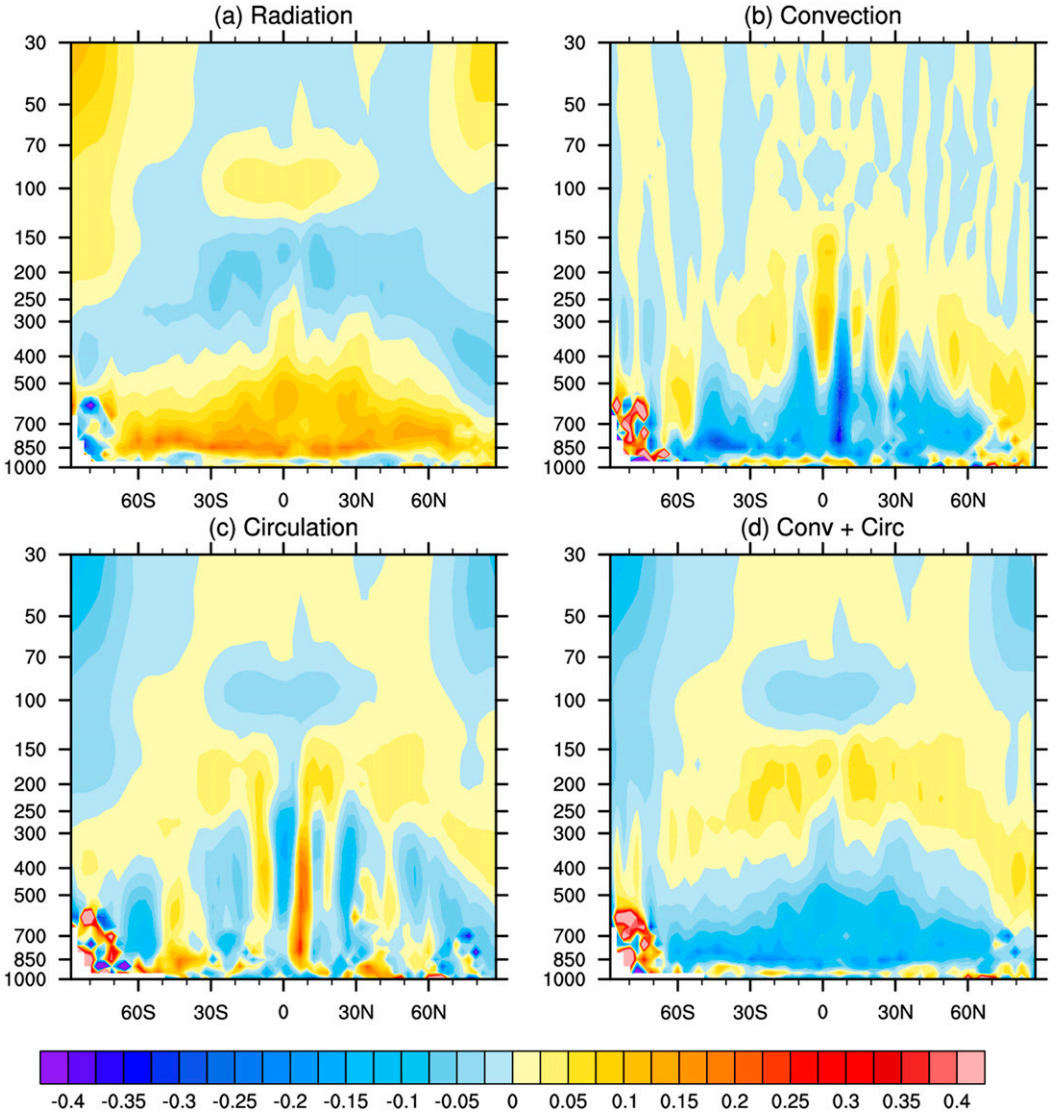

FIG. 13. Heating rate differences between $4 \times CO_2$ and $1 \times CO_2$ experiments in full CAM. (a) Radiative heating rate change, (b) convective heating rate change, (c) circulation heating rate change, and (d) convective plus circulation heating rate change. The component heating rates illustrated here are obtained from the respective modules that compute the temperature tendencies in the GCM integration. Unit: K day^{-1}.

the atmospheric adjustment based on heating rate decomposition.

Acknowledgments. We thank Ming Cai and two anonymous reviewers for the comments and constructive criticisms that helped improve this paper. We acknowledge the funding from the Natural Sciences and Engineering Council of Canada (RGPIN-2019-04511) and the Fonds de Recherché Nature et Technologies of Quebec (FRQNT-NSFC 264835) that supported this research. YW acknowledges the support of the McGill Space Institute Postdoctoral Fellowship.

REFERENCES

Cai, M., and J. Lu, 2009: A new framework for isolating individual feedback processes in coupled general circulation climate models. Part II: Method demonstrations and comparisons. *Climate Dyn.*, **32**, 887–900, https://doi.org/10.1007/s00382-008-0424-4.

Cess, R. D., and Coauthors, 1990: Intercomparison and interpretation of climate feedback processes in 19 atmospheric general circulation models. *J. Geophys. Res.*, **95**, 16 601–16 615, https://doi.org/10.1029/JD095iD10p16601.

Chen, T.-C., M. Yau, and D. J. Kirshbaum, 2018: Assessment of conditional symmetric instability from global reanalysis data. *J. Atmos. Sci.*, **75**, 2425–2443, https://doi.org/10.1175/JAS-D-17-0221.1.

Clough, S., M. Shephard, E. Mlawer, J. Delamere, M. Iacono, K. Cady-Pereira, S. Boukabara, and P. Brown, 2005: Atmospheric radiative transfer modeling: a summary of the AER codes. *J. Quant. Spectrosc. Radiat. Transfer*, **91**, 233–244, https://doi.org/10.1016/j.jqsrt.2004.05.058.

Conley, A., J.-F. Lamarque, F. Vitt, W. Collins, and J. Kiehl, 2013: PORT, a CESM tool for the diagnosis of radiative forcing. *Geosci. Model Dev.*, **6**, 469–476, https://doi.org/10.5194/gmd-6-469-2013.

Cronin, T. W., and K. A. Emanuel, 2013: The climate time scale in the approach to radiative-convective equilibrium. *J. Adv. Model. Earth Syst.*, **5**, 843–849, https://doi.org/10.1002/jame.20049.

Eaton, B., 2011: User's guide to the Community Atmosphere Model CAM-5.1. NCAR, http://www.cesm.ucar.edu/models/cesm1.0/cam/docs/ug5_1/ug.html.

Fels, S., J. Mahlman, M. Schwarzkopf, and R. Sinclair, 1980: Stratospheric sensitivity to perturbations in ozone and carbon dioxide: Radiative and dynamical response. *J. Atmos. Sci.*, **37**, 2265–2297, https://doi.org/10.1175/1520-0469(1980)037<2265:SSTPIO>2.0.CO;2.

Gettelman, A., J. Truesdale, J. Bacmeister, P. Caldwell, R. Neale, P. Bogenschutz, and I. Simpson, 2019: The Single Column Atmosphere Model version 6 (SCAM6): Not a scam but a tool for model evaluation and development. *J. Adv. Model. Earth Syst.*, **11**, 1381–1401, https://doi.org/10.1029/2018MS001578.

Goody, R., and Y. Yung, 1989: Radiation: Theoretical Basis. Oxford University Press, 519 pp.

Hansen, J., M. Sato, and R. Ruedy, 1997: Radiative forcing and climate response. J. Geophys. Res., 102, 6831–6864, https://doi.org/10.1029/96JD03436.

Huang, Y., and Y. Wang, 2019: How does radiation code accuracy matter? *J. Geophys. Res. Atmos.*, **124**, 10 742–10 752, https://doi.org/10.1029/2019JD030296.

——, M. Zhang, Y. Xia, Y. Hu, and S.-W. Son, 2016: Is there a stratospheric radiative feedback in global warming simulations? *Climate Dyn.*, **46**, 177–186, https://doi.org/10.1007/s00382-015-2577-2.

Hurrell, J. W., J. J. Hack, D. Shea, J. M. Caron, and J. Rosinski, 2008: A new sea surface temperature and sea ice boundary dataset for the Community Atmosphere Model. *J. Climate*, **21**, 5145–5153, https://doi.org/10.1175/2008JCLI2292.1.

IPCC, 2013: *Climate Change 2013: The Physical Science Basis*. Cambridge University Press, 1535 pp., https://doi.org/10.1017/CBO9781107415324.

Laliberté, F., and P. Kushner, 2013: Isentropic constraints by midlatitude surface warming on the Arctic midtroposphere. *Geophys. Res. Lett.*, **40**, 606–611, https://doi.org/10.1029/2012GL054306.

Lin, P., and Q. Fu, 2013: Changes in various branches of the Brewer–Dobson circulation from an ensemble of chemistry climate models. *J. Geophys. Res. Atmos.*, **118**, 73–84, https://doi.org/10.1029/2012JB009633.

——, D. Paynter, Y. Ming, and V. Ramaswamy, 2017: Changes of the tropical tropopause layer under global warming. *J. Climate*, **30**, 1245–1258, https://doi.org/10.1175/JCLI-D-16-0457.1.

Lu, J., and M. Cai, 2009: A new framework for isolating individual feedback processes in coupled general circulation climate models. Part I: Formulation. *Climate Dyn.*, **32**, 873–885, https://doi.org/10.1007/s00382-008-0425-3.

Manabe, S., and R. F. Strickler, 1964: Thermal equilibrium of the atmosphere with a convective adjustment. *J. Atmos. Sci.*, **21**, 361–385, https://doi.org/10.1175/1520-0469(1964)021<0361:TEOTAW>2.0.CO;2.

——, and R. T. Wetherald, 1967: Thermal equilibrium of the atmosphere with a given distribution of relative humidity. *J. Atmos. Sci.*, **24**, 241–259, https://doi.org/10.1175/1520-0469(1967)024<0241:TEOTAW>2.0.CO;2.

McLandress, C., D. Plummer, and T. Shepherd, 2014: A simple procedure for removing temporal discontinuities in ERA-Interim upper stratospheric temperatures for use in nudged chemistry-climate model simulations. *Atmos. Chem. Phys.*, **14**, 1547–1555, https://doi.org/10.5194/acp-14-1547-2014.

Merlis, T. M., and M. Henry, 2018: Simple estimates of polar amplification in moist diffusive energy balance models. *J. Climate*, **31**, 5811–5824, https://doi.org/10.1175/JCLI-D-17-0578.1.

Ramaswamy, V., and Coauthors, 2001: Radiative forcing of climate. *Climate Change 2001: The Scientific Basis*. Cambridge University Press, 349–416, J. T. Houghton et al., Eds., https://www.ipcc.ch/site/assets/uploads/2018/03/TAR-06.pdf.

Shell, K. M., J. T. Kiehl, and C. A. Shields, 2008: Using the radiative kernel technique to calculate climate feedbacks in NCAR's Community Atmospheric Model. *J. Climate*, **21**, 2269–2282, https://doi.org/10.1175/2007JCLI2044.1.

Soden, B. J., W. D. Collins, and D. R. Feldman, 2018: Reducing uncertainties in climate models. *Science*, **361**, 326–327, https://doi.org/10.1126/science.aau1864.

Song, X., G. J. Zhang, and M. Cai, 2014: Quantifying contributions of climate feedbacks to tropospheric warming in the NCAR CCSM3. 0. *Climate Dyn.*, **42**, 901–917, https://doi.org/10.1007/s00382-013-1805-x.

Taylor, K. E., R. J. Stouffer, and G. A. Meehl, 2012: An overview of CMIP5 and the experiment design. *Bull. Amer. Meteor. Soc.*, **93**, 485–498, https://doi.org/10.1175/BAMS-D-11-00094.1.

Thuburn, J., and G. C. Craig, 2002: On the temperature structure of the tropical substratosphere. *J. Geophys. Res.*, **107**, 4017, https://doi.org/10.1029/2001JD000448.

Vial, J., J.-L. Dufresne, and S. Bony, 2013: On the interpretation of inter-model spread in CMIP5 climate sensitivity estimates. *Climate Dyn.*, **41**, 3339–3362, https://doi.org/10.1007/s00382-013-1725-9.

Wang, W.-C., and P. B. Ryan, 1983: Overlapping effect of atmospheric H_2O, CO_2 and O_3 on the CO_2 radiative effect. *Tellus*, **35B**, 81–91, https://doi.org/10.3402/tellusb.v35i2.14788.

Zhang, M., and Y. Huang, 2014: Radiative forcing of quadrupling CO_2. *J. Climate*, **27**, 2496–2508, https://doi.org/10.1175/JCLI-D-13-00535.1.